

A matrix isolation and DFT study of the generation and characterization of monomeric vapour phase platinum chlorides

Adam J. Bridgeman^{a,1}, Germán Cavigliasso^{a,b}, Neil Harris^a,
Nigel A. Young^{a,*}

^a Department of Chemistry, The University of Hull, Hull HU6 7RX, UK

^b Department of Chemistry, The University of Cambridge, Cambridge CB2 1EW, UK

Received 20 September 2001; in final form 14 November 2001

Abstract

Molecular platinum monochloride (PtCl) and platinum dichloride (PtCl₂) have been prepared from platinum atoms and chlorine doped argon in a hollow-cathode sputtering device, matrix isolated in solid argon and characterized using electronic, infrared and X-ray absorption spectroscopies together with high level DFT calculations. © 2002 Elsevier Science B.V. All rights reserved.

1. Introduction

The information in the literature concerning the vapour phase composition above heated platinum chlorides and platinum heated in the presence of chlorine appears confusing and contradictory. Schäfer and co-workers [1–3] first identified Pt₆Cl₁₂ mass spectrometrically in the vapour above heated platinum(II) chloride and confirmed, using equilibrium measurements, that Pt₆Cl₁₂ is the only Pt–Cl vapour species above heated β-PtCl₂ up to ca. 600 °C [4]. The reaction of platinum with

chlorine has also been studied by Schäfer and co-workers [5,6] and at temperatures below 650 °C the principal platinum containing vapour species is Pt₆Cl₁₂, whilst at higher temperatures, PtCl₃ (ca. 700 °C) and then PtCl₂ (700–1000 °C) become the dominant platinum vapour compounds. Landsberg and Schaller [7] have also identified the presence of Pt₃Cl₃ in the reaction of platinum and chlorine from vapour pressure measurements. Makarov et al. [8] in recent mass spectrometric experiments observed the reverse to Schäfer and reported that when hydrated H₂PtCl₆ was heated to only 100–175 °C, PtCl₄ was the major platinum vapour species, and that between 175 and 250 °C this was replaced by PtCl₂. At these temperatures they noted that the vapour pressure of Pt₆Cl₁₂ would be so low as to be unobservable in their experiments. In all cases Cl₂ is also found to be a

* Corresponding author. Fax: +44-1482-466410.

E-mail addresses: a.j.bridgeman@hull.ac.uk (A.J. Bridgeman), n.a.young@hull.ac.uk (N.A. Young).

¹ Also corresponding author.

major component of the vapour phase due to decomposition, and Makarov et al. [8] calculate that at the temperatures of their study the vapour pressure of Cl_2 is about 30 times that of PtCl_2 . There appear to be no spectroscopic investigations of the vapour above heated platinum chlorides.

Due to the uncertainty of the vapour composition above the heated platinum chlorides we have prepared monomeric platinum chlorides using the reaction of chlorine with platinum atoms trapped in argon matrices. Using this approach and in conjunction with high-level DFT calculations we have generated and characterized monomeric PtCl and PtCl_2 for the first time.

2. Experimental and computational methods

The platinum atoms were generated in a hollow-cathode sputtering device based on the design of Green and Reedy [9] which has been described in detail previously [10]. The platinum hollow cathode (platinum foil (Goodfellows, 99.99% 25 μm) inside a hollow copper screw) was mounted in a water cooled and electrically isolated metal flange to which the glass vacuum jacket containing the anode and gas inlet system were connected. The platinum anode was mounted on an adjustable drive (modified Young's PTFE tap) and held centrally in the platinum cathode by a thin silica tube. The flow rate of the discharge gas through the sputtering device was controlled by PTFE capillary valves (Young's) and was sufficient for it to act as the matrix gas as well. The gas mixtures were prepared using standard manometric procedures. The sputtering device was operated at ca. 600–700 V and 15 mA by an Ion-Tech DC power supply.

IR spectra were recorded using a Bruker IFS66 FTIR spectrometer equipped with KBr (MIR) and 6 μm Mylar (FIR) beamsplitters, and DTGS detectors. The vacuum shroud used CsI windows and had a base pressure of ca. 2×10^{-7} mbar before the APD DE204SL Displex closed cycle helium cryostat, (base temperature of ca. 10 K) was turned on. The UV–Vis–NIR spectra were recorded using a Varian Cary 5E spectrometer, with a similar vacuum and pumping regime, except that

CaF_2 windows were used. The Pt L_3 -edge X-ray absorption spectra were collected in fluorescence mode (Canberra 13 element SSD detector) on station 9.2 of the Daresbury Laboratory SRS (operating at 2 GeV with circulating currents of ca. 200 mA) using a Si(220) double crystal monochromator detuned by ca. 50% to remove harmonic contamination. Fourteen spectra were collected for each matrix sample, averaged and calibrated using the first maximum in the first derivative of the Pt L_3 -edge of Pt foil (11 564 eV [11]). Background subtraction was carried out using PAXAS [12] by fitting the pre-edge region to a quadratic polynomial, subtracting this from the data and approximating the atomic component of the post-edge region with a high (typically sixth) order polynomial. This approximation was optimized in order to minimize the low- r features in the Fourier transforms by an iterative process, although it should be noted that atomic XAFS features may be expected in this part of the FT [13]. Fitting of the experimental data was carried out with EXCURV98 [14] making use of multiple scattering curved wave theory, a von-Barth ground state and a Hedin–Lundqvist exchange potential.

Density functional (DF) calculations were carried out with the ADF program (ADF2000.02) [15] using the VWN form of the LDA and the BP86 gradient corrections. STO basis sets of triple- ζ quality incorporating frozen cores up to 2p for chlorine and up to 4f for Pt and the ZORA relativistic approach [15] were utilized. Single point calculations were also performed with ZORA plus spin–orbit coupling. SVFF calculations were carried out using the Wilson GF method within SOTONVIB [16].

3. Results and discussion

The electronic absorption spectrum of the products in an argon matrix obtained when Pt was sputtered with neat argon is shown in Fig. 1a. The spectral features are in very good agreement with those for Pt atoms isolated in argon matrices [17,18], with no evidence for the formation of dimers or higher order multimers [19] thus indicating that the hollow cathode device is an excellent

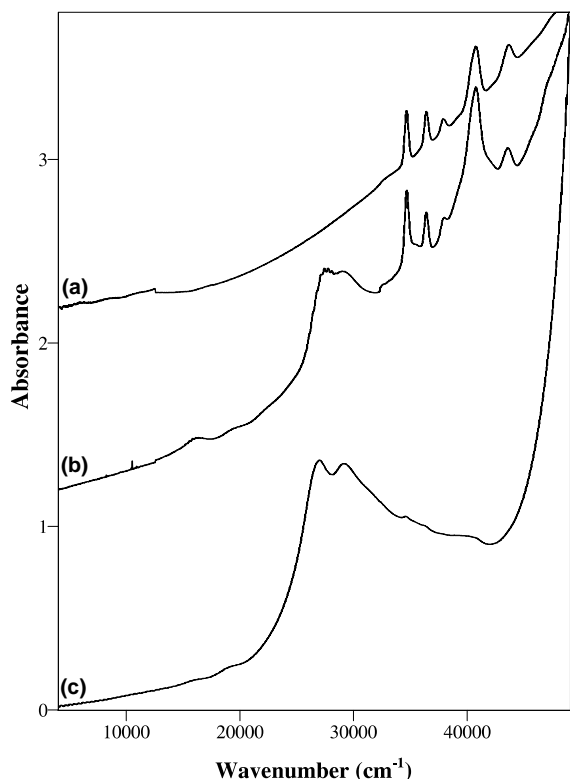


Fig. 1. Electronic absorption spectra of the products matrix isolated from a Pt hollow-cathode sputtered with (a) neat argon, (b) argon doped with 1% Cl_2 , and (c) argon doped with 5% Cl_2 (spectra offset for clarity).

source for matrix isolated atoms. When the argon discharge gas was doped with 1% Cl_2 the spectra (Fig. 1b) contained new features, some of which displayed vibrational fine structure, in addition to those of the Pt atoms or Cl_2 at $30\,500\text{ cm}^{-1}$. When the argon was doped with 5% Cl_2 (Fig. 1c) there were fewer new bands in addition to those of Cl_2 and only negligible signs of any Pt atoms, indicating the formation of fewer PtCl_n species than for the 1% Cl_2 doped case. The two bands at ca. $27\,000$ and $29\,000\text{ cm}^{-1}$ have the same relative intensity in the spectra using both 1% and 5% Cl_2 doped Ar and are assigned to the major PtCl_n species formed in both cases. In addition to these two relatively intense bands there is also a weak feature at ca. $19\,150\text{ cm}^{-1}$ in both sets of spectra, which can also be assigned to this major species. In the spectra from the 1% Cl_2/Ar discharge mixture

the intense band at $27\,000\text{ cm}^{-1}$ displayed vibrational fine structure with a spacing of ca. 320 cm^{-1} , and on the weak band at $19\,150\text{ cm}^{-1}$ there is the indication of vibrational fine structure with a similar interval. In addition to these three bands assigned to charge-transfer transitions in the major species there is a broad band at $16\,040\text{ cm}^{-1}$ which appears to consist of two vibrational progressions of ca. 260 cm^{-1} , separated by ca. 350 cm^{-1} , which are assigned to a minor PtCl_n species. In addition, there are some very sharp and weak features at $10\,850$, $10\,640$, $10\,450$ and 8215 cm^{-1} that cannot be assigned with certainty. Therefore, the electronic absorption spectra indicate the formation of one species using 5% Cl_2/Ar , and the formation of this as well as a second, minor species with 1% Cl_2/Ar discharge gas.

The matrix infrared spectrum (Fig. 2a) obtained when the platinum was sputtered with 5% Cl_2/Ar contained one broad band at 430 cm^{-1} with no

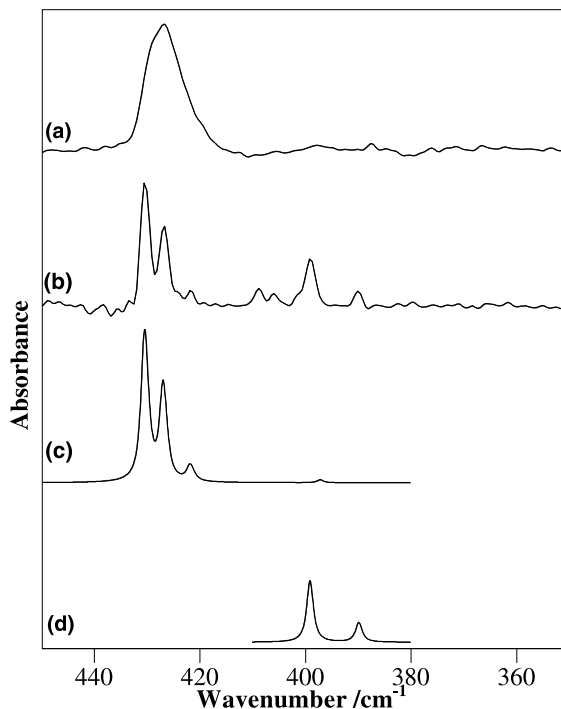


Fig. 2. Infrared spectra of the products matrix isolated from a Pt hollow-cathode sputtered with (a) argon doped with 5% Cl_2 , (b) argon doped with 0.5% Cl_2 . SVFF calculated spectra for (c) linear PtCl_2 and (d) PtCl .

Table 1
Observed and SVFF calculated frequencies (cm^{-1}) for PtCl_2 and PtCl

	Observed		Calculated					
	ν_3	ν_1	180°		150°		130°	
			ν_3	ν_1	ν_3	ν_1	ν_3	ν_1
$\text{Pt}^{35}\text{Cl}_2$	430.4	–	430.4	400.0	430.4	403.0	430.4	406.5
$\text{Pt}^{35}\text{Cl}^{37}\text{Cl}$	426.8	–	426.8	393.8	426.8	396.8	426.8	400.3
$\text{Pt}^{37}\text{Cl}_2$	421.7	–	421.8	389.0	421.6	392.2	421.3	396.0
Pt^{35}Cl		399.1	399.1					
Pt^{37}Cl		390.2	389.9					

¹⁹⁵Pt used for all calculations.

PtCl_2 : 180° $f_r = 3.053 \text{ mdyne } \text{Å}^{-1}$, $f_{rr} = 0.2441 \text{ mdyne } \text{Å}^{-1}$; 150° $f_r = 3.064 \text{ mdyne } \text{Å}^{-1}$, $f_{rr} = 0.2043 \text{ mdyne } \text{Å}^{-1}$; 130° $f_r = 3.074 \text{ mdyne } \text{Å}^{-1}$, $f_{rr} = 0.1260 \text{ mdyne } \text{Å}^{-1}$.

PtCl : $f_r = 2.783 \text{ mdyne } \text{Å}^{-1}$.

resolvable isotopic fine structure. With a more dilute discharge mixture (0.5% Cl_2/Ar), the band at 430 cm^{-1} was resolved into a 9:6:1 triplet (Fig. 2b) characteristic of a vibrational mode of a dichloride. The isotopic structure from the Pt isotopes was not resolved, as to be expected. Using the outermost isotopic bands (430.4 and 421.7 cm^{-1}) in a SVFF calculation gives a bond angle of 163° for a PtCl_2 molecule which, due to the insensitivity of the sine function near 90° , can be regarded as indicative of a linear geometry [20]. Although the position of the central component at 426.8 cm^{-1} arising from the $\text{Pt}^{35}\text{Cl}^{37}\text{Cl}$ isotopomer allows for an estimate of 393.8 cm^{-1} to be made for the position of the symmetric stretching mode, this will be too weak to be observed in the spectra. The data from these calculations are given in Table

1, and the SVFF calculated spectrum for linear PtCl_2 is shown in Fig. 2c. Therefore, the bands at 430 cm^{-1} are assigned to the asymmetric stretching mode of linear PtCl_2 . In addition to this set of bands, weaker features were also present in the spectra. Of these, the two at 399.1 and 390.2 cm^{-1} have a frequency and intensity ratio characteristic of a vibrational mode of a monochloride. The SVFF calculated spectrum of PtCl is shown in Fig. 2d and confirms the assignment. Even weaker features at 408.9 and 406.0 cm^{-1} are most likely due to a matrix site effect of the bands at 430 cm^{-1} as is often observed for metal dichlorides in argon matrices [20].

Table 2 lists the DFT calculated frequencies and IR intensities for PtCl , PtCl_2 , PtCl_3 , PtCl_4 , and *cis* and *trans*- $\text{PtCl}_2(\text{NH}_3)_2$ complexes. For the am-

Table 2
DFT calculated ¹⁹⁵Pt-³⁵Cl frequencies (cm^{-1}) and IR intensities (km mol^{-1}) for PtCl , PtCl_2 , PtCl_3 , PtCl_4 and *cis* and *trans*- $\text{PtCl}_2(\text{NH}_3)_2$

			ν_s	ν_{as}	δ
PtCl	$^2\Pi$	$\text{C}_{\infty v}$	386 (12)	–	
PtCl_2 (bent)	1A_1	C_{2v}	399 (5)	415 (27)	58 (2)
PtCl_2 (linear)	$^3\Sigma_g^-$	$\text{D}_{\infty h}$	389 (0)	419 (57)	79 (0)
PtCl_3	2B_2	C_{2v}	307 (0), 341 (18)	382 (26)	60 (1) b_1 , 91 (3) b_2 , 90 (1) b_2
PtCl_4	$^3A_{2g}$	D_{4h}	359 (0) a_{1g} , 333 (0) b_{1g}	368 (290) e_u	36 (0) b_{2u} , 104 (1) a_{2u} , 166 (0) b_{2g} , 167(0)
<i>cis</i> - $\text{PtCl}_2(\text{NH}_3)_2$ ^a	1A_1	C_{2v}	344 (24)	331 (24)	146 (0)
<i>trans</i> - $\text{PtCl}_2(\text{NH}_3)_2$ ^a	1A_g	C_{2h}	317 (0)	330 (52)	131 (11)

^a The experimental Pt–Cl frequencies are 326 (ν_s) and 318 (ν_{as}) cm^{-1} for *cis*- $\text{PtCl}_2(\text{NH}_3)_2$ and 327 (ν_s) cm^{-1} for *trans*- $\text{PtCl}_2(\text{NH}_3)_2$ [21,22,30].

mine complexes, the agreement with experimental IR and Raman frequencies [21,22,30] is very good, suggesting that the results for the simpler halide molecules should be reliable. The experimental band at 430.4 cm^{-1} is consistent with the values for PtCl_2 in either the ${}^3\Sigma_g^-$ or 1A_1 state. However, the position of the DFT calculated frequencies for the symmetric modes are in much better agreement with the linear rather than bent geometry for PtCl_2 . The calculated frequency for PtCl at 33 cm^{-1} lower than that for ν_{as} of PtCl_2 , together with a consistent offset between observed and calculated values, confirms the assignment of the doublet at 399.1 and 390.2 cm^{-1} to PtCl . The values for PtCl_3 and PtCl_4 appear to be too low with PtCl_3 expected to exhibit two bands. The experimental and calculated vibrational spectra thus indicate that PtCl_2 is formed exclusively in a 5% Cl_2/Ar discharge whereas lower chlorine concentrations results in both PtCl and PtCl_2 being formed, in good agreement with the electronic absorption data.

X-ray absorption fine structure (XAFS) spectroscopy provides local structural information around the platinum. A 5% Cl_2/Ar discharge gas was used to ensure only one PtCl_n species was formed and to minimize the proportion of unreacted Pt atoms as XAFS provides an average environment of all the Pt species present. Fig. 3 shows the XANES data for K_2PtCl_6 and K_2PtCl_4 diluted in BN at 25°C as well as the matrix isolated sputtered products using both neat Ar and 5% Cl_2 doped Ar. Although the edge position and edge shifts of XANES data are often useful in oxidation state determination, this is less useful for L_3 -edge data because the edge region is dominated by the intense ‘white line’ arising from $2p^65d^n$ to $2p_{1/2}^2 2p_{3/2}^3 5d^{n+1}$ transitions. The position of this white line will be affected by the change in the energies of the $2p$ core states and the $5d$ valence orbitals in the different coordination geometries as much as the change in the formal oxidation state. In the past we have noted that the Ni K-edge position for linear nickel dihalides in cryogenic matrices is higher than that for either square planar, tetrahedral or octahedral model compounds [23]. However, the intensity of the white line is very informative as it is related to the number of holes

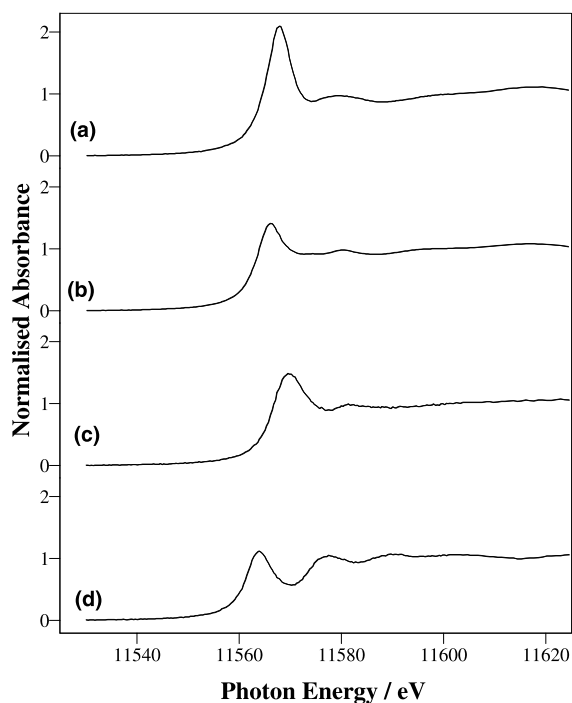


Fig. 3. Pt L_3 edge XANES spectra for (a) K_2PtCl_6 diluted in BN at 298 K, (b) K_2PtCl_4 diluted in BN at 298 K, (c) products matrix isolated from a Pt hollow-cathode sputtered with 5% Cl_2 doped Ar and (d) products matrix isolated from a Pt hollow-cathode sputtered with neat Ar.

in the $5d$ valence orbitals and hence oxidation state of the platinum [24], and the spectra of K_2PtCl_6 and K_2PtCl_4 (Fig. 3a,b) clearly show that the intensity of the white line for K_2PtCl_4 is less than that of K_2PtCl_6 . The intensity of the white line in the spectrum of the products when Pt was sputtered with 5% Cl_2 (Fig. 3c) is very similar to that of K_2PtCl_4 , confirming the formation of a Pt^{II} compound. The lack of any significant Pt atom concentration is shown by comparison with the spectrum obtained from the products sputtered with neat Ar (Fig. 3d).

The EXAFS part of the spectrum can be used to obtain inter- and intra-molecular distances from the Pt. In order to confirm the accuracy of the Pt–Cl distances, Pt L_3 -edge data were also collected for K_2PtCl_4 and K_2PtCl_6 which yielded Pt–Cl distances of $2.31(2)\text{ \AA}$ for K_2PtCl_4 and $2.32(2)$ for K_2PtCl_6 in excellent agreement with a very recent EXAFS study [25] as well as single crystal X-ray

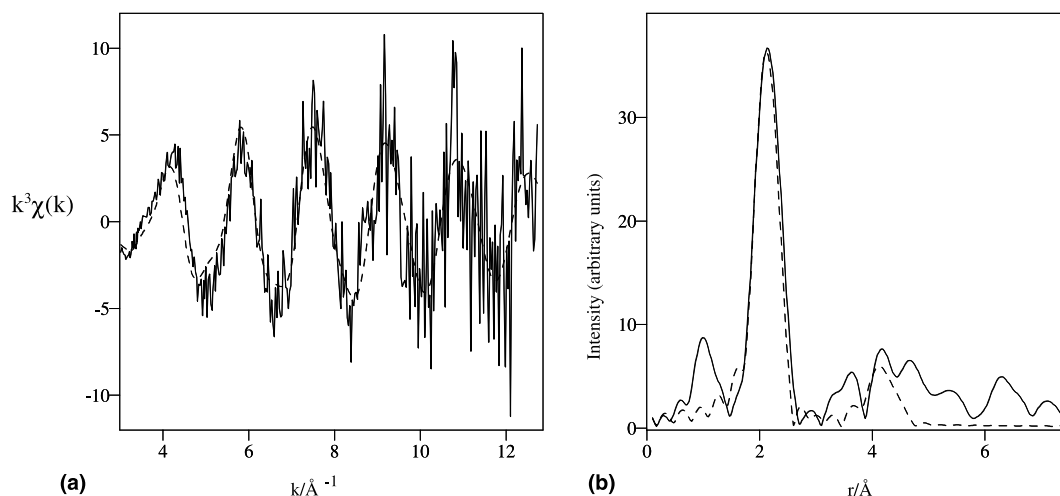


Fig. 4. Pt L₃-edge EXAFS (a) and Fourier transform (b) of the products matrix isolated from a Pt hollow-cathode sputtered with 5% Cl₂ doped Ar. Solid line, experimental data, dotted line, curved wave multiple scattering theory for linear PtCl₂.

data [26,27]. The Pt L₃-edge data of the products when Pt was sputtered with 5% Cl₂/Ar are shown in Fig. 4 and Table 3. The data is fairly noisy due to the limited Ar penetration depth at these energies (ca. 60 μm), which meant that it had to be truncated at ca. 13 Å⁻¹. The FT of the EXAFS data reveals one significant peak due to a Pt–Cl

interaction of 2.19(2) Å. This is 0.12 Å shorter than that observed in either K₂PtCl₄ or K₂PtCl₆, and confirms that the spectrum is indeed arising from a low coordination number compound, as we have observed a similar shortening of metal–halogen bond lengths in matrix isolated NiBr₂ [23]. When the Cl occupation number was included in

Table 3

Refined XAFS parameters^a for K₂PtCl₄, K₂PtCl₆ and matrix isolated products when Pt cathode is sputtered with 5% Cl₂/Ar

	$r_{\text{Pt-Cl}}^c$ (Å)	$2\sigma^2$ ^f (Å ²)	E_f^g (eV)	FI ^h	R^i
K ₂ PtCl ₄ (298 K)					
X-ray diffraction ^b	2.309				
Pt L ₃ -edge XAFS ^c	2.309(3)	0.0068(3)	-10.8	2.72	25.80
KPtCl ₆ (298 K)					
X-ray diffraction ^d	2.311				
Pt L ₃ -edge XAFS ^c	2.322(4)	0.0061(4)	-11.3(8)	4.73	31.88
Pt products sputtered with 5% Cl/Ar (10 K)					
Pt L ₃ -edge XAFS	2.193(97)	0.0059(12)	-7.6(2)	17.3	58.07

^a Standard deviation in parentheses.

^b Ref. [26].

^c This work.

^d Ref. [27].

^e Estimated systematic errors in XAFS bond lengths are ±1.5% for well-defined co-ordination shells.

^f $2\sigma^2$ is the Debye–Waller factor.

^g E_f is a single refined parameter to reflect differences in the theoretical and experimental Fermi levels.

^h $FI = \sum_i [(Z_i^T - \chi_i^E)k_i^3]^2$.

ⁱ $R = [\int |\chi^T - \chi^E|k^3 dk / \int |\chi^E|k^3 dk] \times 100\%$.

the refinement, a value of 2.3 was obtained. Whilst this is a little large for PtCl₂, coordination numbers are notoriously hard to determine accurately using EXAFS, especially for noisy data. Features in the FTs at approximately twice the Pt–Cl distance would confirm a linear geometry [23,25,28], and the multiple scattering pathways giving rise to these are included in the final refinement shown in Fig. 4. Whilst there is the probability of such a feature in the data, the inherent noise makes it very hard to identify unambiguously.

The DFT calculated structures for PtCl, PtCl₂, PtCl₃, PtCl₄ and *cis* and *trans*-PtCl₂(NH₃)₂ are given in Table 4. The BP86 results for the ammine complexes show extremely good agreement with crystallographically determined geometries [29], with a slight improvement upon recently reported calculations [30], suggesting again that the computational method is reliable for these heavy metal complexes. The calculated bond lengths for PtCl_{*n*} show an increase with oxidation state and coordination number. The best agreement with the EXAFS values is for linear PtCl₂, although the values for bent PtCl₂ and PtCl are very similar. The bond lengths in the T-shaped PtCl₃ and square planar PtCl₄ molecules are somewhat longer.

Linear PtCl₂ is predicted to be 59 kJ mol⁻¹ more stable at the LDA level and 64 kJ mol⁻¹ at the BP86 level than the bent form. Inclusion of spin–orbit coupling in the ZORA calculations decreases these values somewhat to 37 and 34 kJ mol⁻¹, respectively. Siegbahn [31] predicts a linear geometry for PdF₂ and a highly bent (98°)

geometry for PdCl₂. Wesendrup and Schwerdtfeger [32] predict a linear geometry for PtF₂. The XANES and EXAFS data and the DFT structures and energies are thus consistent with the vibrational and electronic absorption data and suggest formation of linear PtCl₂ when Pt foil is sputtered with a 5% Cl₂/Ar gas mixture.

The linear d⁸PtCl₂ molecule is predicted to have ³Σ_g⁻ ground state for the δ_g⁴σ_g²π_g² configuration identical to that predicted for NiCl₂ [33]. The bent molecule has a ¹A₁ ground state which can be thought of as arising from a Renner–Teller splitting of the low-spin ¹Π_g state of δ_g⁴σ_g²π_g². The ¹A₁ state has double occupation of the resulting a₂ orbital with the b₂ component of the π_g level empty. The (a₂)² configuration greatly reduces the out-of-plane π bonding but the in-plane bonding is enhanced through d–p hybridization. Through mixing with Pt 6p_y, the d_{yz} orbital becomes strongly directed towards the ligands so that the anti-bonding b₂ orbital is destabilized. The bonding is thus increased even though the out-of-plane component is reduced. The square planar geometry of PtCl₄²⁻ leads to a single strongly anti-bonding d-orbital and hence to a large LFSE for the low spin d⁸ configuration. The bent PtCl₂ geometry can be considered as one half of a square planar molecule and similarly leads to a single strongly anti-bonding d-orbital and high LFSE. The preference for the linear or bent geometry thus rides on the familiar balance between the electron pairing energy and the bonding.

Although experimental evidence shows the isolation of PtCl and PtCl₂, it is noteworthy that

Table 4
DFT calculated structures for PtCl, PtCl₂, PtCl₃, PtCl₄ and *cis* and *trans*-PtCl₂(NH₃)₂

		Symmetry	Pt–Cl bond lengths (Å)		Bond angle (°)	
			LDA	BP86	LDA	BP86
PtCl	² Π	C _{∞v}	2.151	2.181	–	–
PtCl ₂	¹ A ₁	C _{2v}	2.144	2.183	130	130
PtCl ₂	³ Σ _g ⁻	D _{∞h}	2.148	2.187	180	180
PtCl ₃	² B ₂	C _{2v}	2.228 (×2)	2.238 (×2)	100 (×2)	101 (×2)
			2.216	2.221	160	157
PtCl ₄	³ A _{2g}	D _{4h}	2.266	2.275	90	90
<i>cis</i> -PtCl ₂ (NH ₃) ₂ ^a	¹ A ₁	C _{2v}	2.273	2.315	96	96
<i>trans</i> -PtCl ₂ (NH ₃) ₂ ^a	¹ A _g	C _{2h}	2.292	2.337	178	178

^a The experimental Pt–Cl bond lengths of *cis* and *trans*-PtCl₂(NH₃)₂ are 2.33 and 2.32 Å, respectively [29].

PtCl₃ and PtCl₄ are actually calculated to be more stable than PtCl₂. Decomposition of PtCl₃ to PtCl₂ + 1/2Cl₂ and PtCl₄ to PtCl₂ + Cl₂ are predicted to require 55 and 150 kJ mol⁻¹, respectively. Decomposition of PtCl₂ to PtCl + 1/2Cl₂ is predicted to require 240 kJ mol⁻¹. The DF calculations thus predict that linear PtCl₂ is formed as the kinetic product in the reaction of Pt atoms and Cl₂ under these experimental conditions.

4. Conclusions

A hollow-cathode sputtering device is an excellent source of matrix isolated atoms when used with neat argon, and new species can be formed when the argon is doped with chlorine. The use of matrix isolation electronic absorption spectroscopy, infrared spectroscopy and X-ray absorption spectroscopy in conjunction with high level DFT calculations has resulted in the first observation and characterization of molecular monomeric platinum monochloride and platinum dichloride. This should assist in the spectroscopic characterization of the vapour above heated platinum chlorides.

Acknowledgements

We gratefully acknowledge: the gift of the sputtering device from Prof. Ian Beattie; the financial support of the EPSRC (studentships to GC and NH, SRS beamtime), the University of Hull, the Cambridge Overseas Trust and Selwyn College (Cambridge); the Director of Daresbury Laboratory for access to the synchrotron; and the Computational Chemistry Working Party for access to computational facilities in the Rutherford Appleton Laboratory.

References

- [1] H. Schäfer, U. Wiese, K. Rinke, K. Brendel, *Angew. Chem. Int. Ed. Engl.* 6 (1967) 253.
- [2] U. Wiese, H. Schäfer, H.G. v. Schnering, C. Brendel, K. Rinke, *Angew. Chem. Int. Ed. Engl.* 9 (1970) 158.
- [3] H. Schäfer, U. Wiese, H. Rabeneck, *Z. Anorg. Allg. Chem.* 513 (1984) 157.
- [4] H. Schäfer, *Z. Anorg. Allg. Chem.* 415 (1975) 217.
- [5] U. Wosiewitz, H. Schäfer, *J. Less-Common Met.* 32 (1973) 389.
- [6] H. Schäfer, U. Wosiewitz, *Z. Anorg. Allg. Chem.* 415 (1975) 202.
- [7] A. Landsberg, J.L. Schaller, *J. Less-Common Met.* 23 (1971) 195.
- [8] E.V. Makarov, V.A. Bryukvin, V.K. Tagirov, *Russ. J. Non-Ferrous Met.* 38 (1997) 35.
- [9] D.W. Green, G.T. Reedy, *J. Chem. Phys.* 69 (1978) 544.
- [10] I.R. Beattie, P.J. Jones, K.R. Millington, A.D. Willson, *J. Chem. Soc., Dalton Trans.* (1988) 2759.
- [11] X-ray data booklet, Center for X-ray Optics and Advanced Light Source, Lawrence Berkeley National Laboratory, University of California, Berkeley, CA USA, 2001.
- [12] N. Binsted, PAXAS, Program for the Analysis of X-Ray Absorption Spectra, University of Southampton, 1988.
- [13] W.E. O'Grady, X. Qian, D.E. Ramaker, *J. Phys. Chem. B* 101 (1997) 5624.
- [14] N. Binsted, EXCURV98, CCLRC Daresbury Laboratory Computer Program, 1998.
- [15] G. te Velde, F.M. Bickelhaupt, E.J. Baerends, C. Fonseca Guerra, S.J.A. van Gisbergen, J.G. Snijders, T. Ziegler, *J. Comput. Chem.* 22 (2001) 931, and references therein.
- [16] I.R. Beattie, N. Cheetham, M. Gardner, D.E. Rogers, *J. Chem. Soc. A* (1971) 2240.
- [17] D.H.W. Carstens, W. Brashear, D.R. Eslinger, D.M. Gruen, *Appl. Spectrosc.* 26 (1972) 184.
- [18] W. Klotzbücher, G.A. Ozin, *Inorg. Chem.* 15 (1976) 292.
- [19] K. Jansson, R. Scullman, *J. Mol. Spectrosc.* 61 (1976) 299.
- [20] I.R. Beattie, P.J. Jones, N.A. Young, *Chem. Phys. Lett.* 177 (1991) 579.
- [21] P.J. Hendra, *Spectra. Chim. Acta* 23A (1967) 1275.
- [22] L.A. Degen, A.J. Rowlands, *Spectra. Chim. Acta* 47A (1991) 1263.
- [23] N.A. Young, *J. Chem. Soc., Dalton Trans.* (1996) 249.
- [24] A.L. Ankudinov, J.J. Rehr, S.R. Bare, *Chem. Phys. Lett.* 316 (2000) 495.
- [25] R. Ayala, E.S. Marcos, S. Díaz-Moreno, V.A. Solé, A. Muñoz-Páez, *J. Phys. Chem. B* 105 (2001) 7588.
- [26] D.H. Templeton, L.K. Templeton, *Acta Crystallogr. A* 41 (1985) 365.
- [27] R. Restori, D. Schwarzenbach, *Acta Crystallogr. A* 52 (1996) 369.
- [28] A. van der Gaauw, O.M. Wilkin, N.A. Young, *J. Chem. Soc., Dalton Trans.* (1999) 2405.
- [29] G.H.W. Milburn, M.R. Truter, *J. Chem. Soc. A* (1966) 1609.
- [30] R. Wysokinski, D. Michalska, *J. Comput. Chem.* 22 (2001) 901.
- [31] P.E.M. Siegbahn, *Theor. Chim. Acta* 87 (1994) 441.
- [32] R. Wesendrup, P. Schwerdtfeger, *Inorg. Chem.* 40 (2001) 3351.
- [33] A.J. Bridgeman, *J. Chem. Soc. Dalton Trans.* (1996) 2601.